Interface Focus
doi:10.1098/rsfs.2010.0048
Published online

euHeart: personalized and integrated cardiac care using patient-specific cardiovascular modelling

Nic Smith[1,2,*], Adelaide de Vecchi[1], Mathew McCormick[2], David Nordsletten[1], Oscar Camara[3,4], Alejandro F. Frangi[3,4,5], Hervé Delingette[6], Maxime Sermesant[6], Jatin Relan[6], Nicholas Ayache[6], Martin W. Krueger[7], Walther H. W. Schulze[7], Rod Hose[8], Israel Valverde[1], Philipp Beerbaum[1], Cristina Staicu[8], Maria Siebes[9], Jos Spaan[9], Peter Hunter[10], Juergen Weese[11], Helko Lehmann[11], Dominique Chapelle[12] and Reza Rezavi[1]

[1]*Imaging Sciences and Biomedical Engineering Division, St Thomas' Hospital, King's College London, London, UK*
[2]*Computing Laboratory, University of Oxford, Oxford, UK*
[3]*Center for Computational Imaging and Simulation Technologies in Biomedicine (CISTIB), Universitat Pompeu Fabra, Barcelona, Spain*
[4]*Networking Biomedical Research Center on Bioengineering, Biomaterials and Nanomedicine (CIBER-BBN), Barcelona, Spain*
[5]*Institució Catalana de Recerca i Estudis Avançats (ICREA), Barcelona, Spain*
[6]*INRIA Sophia-Antipolis, Sophia Antipolis Cedex, France*
[7]*Institute of Biomedical Engineering, Karlsruhe Institute of Technology (KIT), Karlsruhe, Germany*
[8]*Department of Cardiovascular Science, University of Sheffield, Sheffield, UK*
[9]*Academic Medical Center Amsterdam, Amsterdam, The Netherlands*
[10]*Bioengineering Institute, University of Auckland, Auckland, New Zealand*
[11]*Philips Research Laboratories, Eindhoven, The Netherlands*
[12]*INRIA Paris-Rocquencourt, Paris, France*

The loss of cardiac pump function accounts for a significant increase in both mortality and morbidity in Western society, where there is currently a one in four lifetime risk, and costs associated with acute and long-term hospital treatments are accelerating. The significance of cardiac disease has motivated the application of state-of-the-art clinical imaging techniques and functional signal analysis to aid diagnosis and clinical planning. Measurements of cardiac function currently provide high-resolution datasets for characterizing cardiac patients. However, the clinical practice of using population-based metrics derived from separate image or signal-based datasets often indicates contradictory treatments plans owing to inter-individual variability in pathophysiology. To address this issue, the goal of our work, demonstrated in this study through four specific clinical applications, is to integrate multiple types of functional data into a consistent framework using multi-scale computational modelling.

Keywords: cardiac modelling; patient specific; multi-scale; virtual physiological human

1. INTRODUCTION

Cardiovascular disease (CVD) is a highly significant contributor to loss of quality and quantity of life within Europe, where each year CVD causes over 4.35 million deaths, including nearly half of all non-accidental deaths [1]. It is most commonly a consequence of diseases such as coronary artery disease (CAD), congestive heart failure (HF) and cardiac arrhythmias. Thus, the early detection and prediction of the progression of CVD are key requirements towards improved treatment, and reduction in mortality and morbidity.

The diversity and quantity of currently available imaging data, including measurements of cardiac wall motion [2], chamber flow patterns [3], coronary perfusion

*Author for correspondence (nicoas.smith@kcl.ac.uk).

One contribution to a Theme Issue 'The virtual physiological human'.

Received 13 December 2010
Accepted 4 March 2011

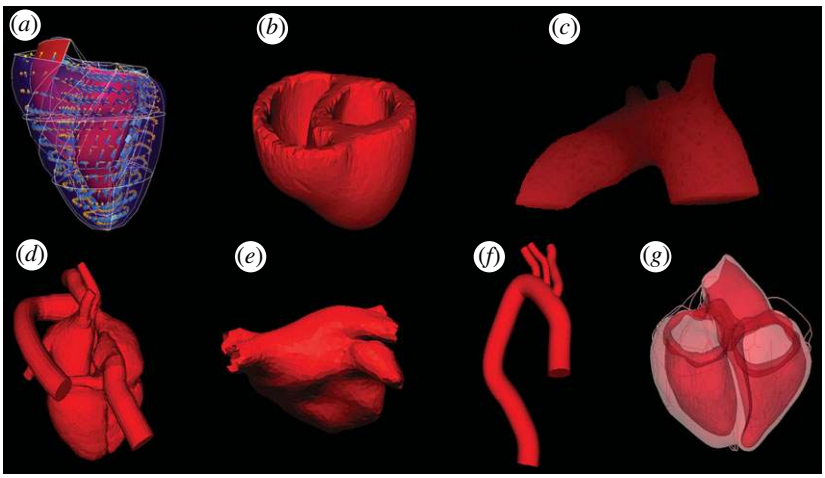

Figure 1. Three-dimensional visualizations of (*a*) Auckland Heart [11], (*b*) INRIA Heart [12], (*c*) INRIA Sophia Aorta, (*d*) Philips Cardiac Atlas [13], (*e*) Philips Left Atrium [14], (*f*) Sheffield Aorta [15] and (*g*) UPF Heart [16].

[4] and electrical mapping [5], present a significant opportunity to improve clinical care of CVD. Similarly, functional measurement of haemodynamic coronary signals results in improved clinical outcome [6]. However, the clinical practice of using population-based metrics derived from separate image sets often indicates contradictory treatment plans owing to inter-subject variability in pathophysiology. Thus, despite advances in imaging and functional measurements, determining optimal treatment strategies for CVD patients remains problematic. To exploit the full value of these technologies, and the combined information content they produce, requires the ability to integrate multiple types of anatomical and functional data into a consistent framework.

An exciting and highly promising strategy for contributing to this integration is through the personalization of bio-physically based mathematical models [7]. The development of such models presents the ability to capture the complex and multi-factorial cause and effect relationships that link underlying pathophysiological mechanisms. This in turn provides the capacity to derive indicators that are not directly observable but play a key mechanistic role in the disease process (for example, tissue stress and measures of pump efficiency to assist treatment decisions). Across international efforts to develop these types of models such as the virtual physiological human (VPH) integrated modelling of the heart is arguably one of the most advanced current examples. As such, it represents an excellent organ system with which to demonstrate the translation of models to clinical application. Specifically, detailed anatomical finite-element (FE)-based models of the heart now accurately represent both cardiac anatomy and detailed microstructure. These mathematical descriptions serve as spatial frameworks for embedding functional cellular models of electrical activation, and the resultant tension generation that produces cardiac contraction. These cell and organ components have been combined through the application of continuum equations to simulate whole-organ cardiac electro-mechanics, perfusion and ventricular fluid dynamics.

However, despite these advances, there remains a significant translational barrier to applying and customizing models for human clinical application. This is because the vast majority of cardiac models are currently developed and validated using data collected from invasive measurements in animal populations under controlled conditions. These models are useful for the demonstration of proof of concept function, development of mechanistic concepts and interpretation of specific animal data. However, there are inherent limitations to such model developments specifically with respect to mimicking disease. Moreover, the relevance of insights gained from such animal models to human health remains difficult to determine [8].

The current challenge is thus to parameterize and personalize these frameworks for humans using the extensive but only minimally invasive clinical measurements. It is this goal of integration and application in patient-specific contexts that is the focus of our 4 year project called euHeart and funded by the European Commission as part of the VPH initiative calls.[1]

The technical work within euHeart is focused on developing the necessary tools to enable clinical applications. This tool development includes the establishment of a library of models of the heart across the euHeart consortium (figure 1) made available via euHeartDB, a web-enabled database [9]. The database implements a dynamic sharing methodology by managing data access and by tracing all applications. In addition to this, euHeartDB establishes a knowledge link with the Physiome Model Repository by linking geometries to CellML models[2] and uses the exFormat—a preliminary version of the interoperable FieldML data format.[3] To enable robust and effective personalization strategies, atlas-based image segmentation techniques [10] are tailored to the specific needs of

[1]euHeart—Personalised and Integrated Cardiac Care: Patient-specific Cardiovascular Modelling and Simulation for In Silico Disease Understanding and Management and for Medical Device Evaluation and Optimization (http://www.euheart.org).
[2]http://www.cellml.org
[3]http://www.fieldml.org

biophysical simulations. In addition, functional parameter estimation techniques are applied to enable the description of cardiac normal and pathological conditions for the major manifestations of CVD. Most of the clinical applications designed within euHeart are prototyped within the GIMIAS[4] [11] application framework environment, which has enabled the integration of tools across different institutions and the implementation of prototypes shared among the participating groups or currently under testing in our clinical sites.

This library of models and tools is currently being integrated into clinical applications to validate the descriptive capabilities of the approach and to demonstrate the plausibility of improving clinical outcomes, when compared with current best practices, for diagnosis, interventional planning and device or treatment optimization. Specifically, models for HF and electrical rhythm disturbances incorporate the description of ion channel kinetics into the organ-level solution of reaction–diffusion equations for computing the activation sequences in ventricular and atrial tissue. These applications also couple the mechanisms for myofilament force generation at the subcellular level to the fluid-mechanical properties of the chamber and heart wall to capture contractile dynamics. Work on CAD incorporates anatomy, perfusion coupled to whole-heart coronary flow. Mechanical contraction and coronary perfusion are also being linked to the constitutive properties of aortic wall tissue for coupling heart function to the pressure-flow behaviour of the circulation [12].

The focus of this article is on the clinical applications within which these tools are now being tested. Specifically, these applications are customizing cardiac resynchronization, coronary revascularization and atrial ablation therapies and device implantation, including left ventricular assist device (LVAD) implantation and valve replacement. The data, modelling methodology and results in each of these areas are summarized in the sections below.

2. CARDIAC RESYNCHRONIZATION THERAPY

One of the targeted clinical applications in euHeart is cardiac resynchronization therapy (CRT), which can relieve HF symptoms by reducing heart dyssynchrony through the implantation of a pacemaker. However, the negative or non-response to CRT rises to 30 per cent [13] owing to challenges in patient selection and pacemaker configurations. This context is a significant issue and focus within the clinical community. The recent update of the official guidelines for CRT from the European Society of Cardiology now includes a number of additional patient groups that were previously omitted [14]. Several research groups are also investigating the testing of new pacing configurations (number and position of leads) in experimental models under fully controlled conditions [15] as well as the different parameters that are related to response to CRT [16]. The hypothesis leading research work on CRT within euHeart is that using patient-specific cardiac models combining the anatomical and functional pre-operative data collected has the potential to provide new insights into the disease and therapy. The generation of these patient-specific models requires a tight, coordinated and collaborative effort between multi-disciplinary teams.

Performing cardiac electromechanical simulations requires building a computer model that can represent the subject's heart morphology with sufficient accuracy. Depending on the amount of clinical data available from the patient, cardiac models can be further personalized to a given pathology or therapy such as CRT. Furthermore, the validation of these computational models needs the extraction of information from images and signals so that they can be compared with simulation results. Patient-specific geometry, tissue properties such as local elasticity or local conductivity, deformation/motion information and details on the microstructure are all desirable to ensure the computational models are as realistic as possible. The main components of the workflow for the generation of the personalized computational models required for the CRT planning platform to be developed in the euHeart project are described in the following. Most of these components are already integrated into a common software framework, GIMIAS [11], which is a workflow-oriented framework extensible through plug-ins, which has been designed for the prototyping of clinical applications requiring streamlined workflows intensively relying on methods of computational imaging and computational physiology.

To support the model development process, new acquisition protocols of cardiac magnetic resonance (MR) have been developed [17] that create three-dimensional whole-heart images allowing automatic or semi-automatic cardiac chamber and coronary sinus segmentation, thus streamlining the clinical workflow. From these data, the cardiac geometry is extracted using automatic and semi-automatic segmentation techniques based on atlases computed from population data [18] or statistical shape models that can be applied to whole-heart computed tomography (CT) or MR images [19]. In addition, the user has manual correction tools if the segmentation is not accurate enough. Functional information such as tissue viability, which is crucial for interventional planning, can also be extracted from late-enhancement magnetic resonance imaging (MRI) [20]. Finally, the coronary venous tree is extracted from vascular segmentation techniques [21] since it will constrain the lead placement, thus providing more realistic device settings in the simulations. The structures segmented in the previous phase (four chambers, scar, coronary tree) from MRI are easily fused into the reference space defined from the three-dimensional whole-heart image, as illustrated in figure 2. In addition, this cardiovascular geometrical information can be overlaid with the X-ray images during the CRT intervention with the pipeline developed at King's College London [17], making the use of the developed tools in clinical routine possible.

[4] http://www.gimias.org

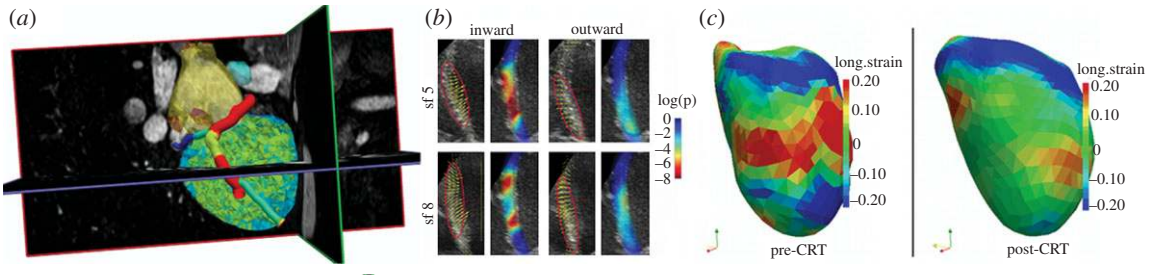

Figure 2. Image analysis for CRT. (*a*) Segmentation of four chambers, scar (yellow triangles in the myocardium) and coronary venous tree from a three-dimensional whole-heart MRI. (*b*) Dyssynchrony analysis from two-dimensional echo data showing significant statistical differences (red map) in the inward and outward septal motion during the isovolumetric contraction period between an atlas of normal subjects and these two (top and bottom) septal flash cases. (*c*) Dyssynchrony analysis from three-dimensional echo data showing the effect of CRT on the longitudinal strain (reduction of large strains, red colour, in the septal wall).

Building on this anatomical framework, a quantitative analysis of the motion/deformation of the heart gives dyssynchrony information, which is particularly relevant for CRT given the aims of restoring synchronous activation of the heart. Towards this goal, three-dimensional echocardiographic images were analysed [22], showing significant differences in strain curves before and after CRT. In addition, algorithms for the quantitative estimation of septal flash [23], a marker of dyssynchrony that has demonstrated a strong relation with a positive response of CRT, based on computing the distance of a CRT candidate to an atlas of deformation normality, have been developed and tested on a large cohort of patients [24]. Finally, this septal flash pattern was also identified from intracardiac electrical mapping data [25], allowing a simple integration of electrical data and motion information.

Using the previous segmentations as geometrical boundary conditions for the models, the FE volumetric meshes required for the simulations were built. Depending on the physiological models used, the nature of these FE meshes and associated boundary conditions will be different, mainly with respect to type and number of elements used. Within the CRT planning platform, it is possible to generate high-resolution tetrahedral meshes from patient-specific segmentations for detailed electrophysiological models. Complementing these tetrahedral meshes, warping techniques have been developed [26] in order to generate high-order patient-specific hexahedral meshes, suitable for mechanical simulations. Finally, these volumetric meshes are further augmented by synthetically adding substructural information relevant for CRT, such as myocardial fibre orientation or the Purkinje system [27], which are boundary conditions significantly changing the outcome of the simulations.

Using these spatial representations, mechanical and electrophysiological cellular models with different levels of complexity (available in the cellML repository) are coupled to tissue activation models and finite deformation mechanics within continuum-based simulation codes optimized for high-performance parallel implementation. Simple electrophysiological models based on Eikonal equations, phenomenological models and more detailed biophysical models are available for the simulation of electrical activation. At the time being, these electrophysiological models are weakly coupled to a nonlinear finite strain elasticity framework for the mechanical simulations. A key step is the personalization of conductivity and stiffness parameters as well as personalizing appropriate boundary conditions, since these variables cannot be measured *in vivo*. From the clinical point of view, realistic and personalized physiological models allow *in silico* tests of different device settings (number and position of leads, chamber delays), which are currently selected suboptimally, as indicated by a lack of consensus in the clinical community. Most of the code has been implemented using open-source platforms such as OpenCMISS[5] and Chaste,[6] which in turn enables collaboration between different research groups. An example of an electrophysiological simulation run with Chaste on a patient-specific geometry extracted from the previous steps is shown in figure 3, with two different pacing configurations. Furthermore, a simple mechanical simulation run with OpenCMISS on the same patient geometry is also illustrated in the figure.

Finally, once electromechanical simulations are obtained, they are post-processed and compared with information and other indices extracted from imaging and signal data, such as deformation fields from echo images, contact or non-contact mapping data or pressure information. This information allows the combination of different parameters derived from imaging, simulation and other patient-specific data (demographics, electrocardiogram (ECG)-derived parameters, etc.) using machine-learning techniques to classify patients in classes with more or less likelihood for a positive response of CRT. Nevertheless, it needs to be pointed out that current models require substantial improvements before being confidently translated into clinical routine. For instance, electrophysiological, mechanics and fluid models are not strongly coupled yet, thus preventing a complete understanding of the different multi-physics phenomena and their interaction in CRT. Furthermore, these models need to be validated in

[5]www.opencmiss.org
[6]www.comlab.ox.ac.uk/Chaste

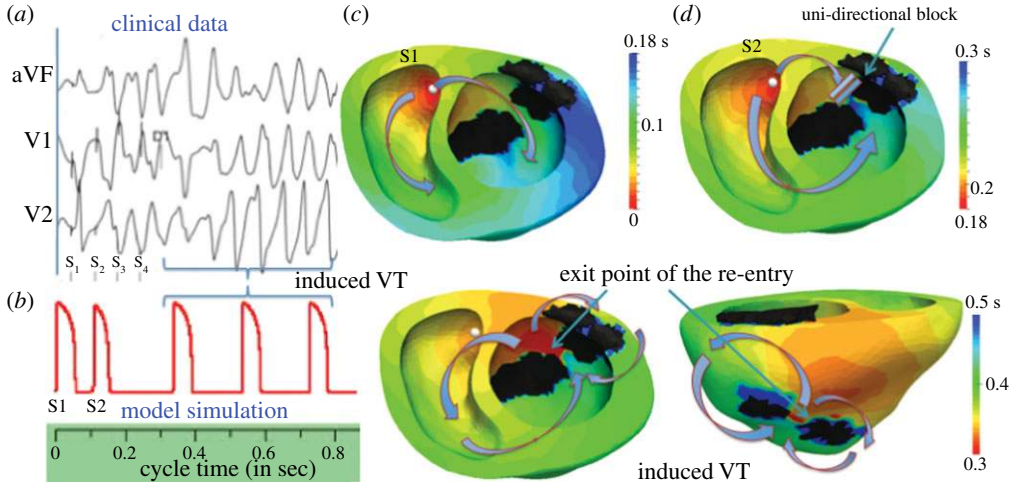

Figure 3. Simulation results of the VT-stim procedure on a three-dimensional biventricular model of the human ventricle using the MS model. The colours show the depolarization time (DT) isochrones. (*a*) A prototype for unipolar electrograms recorded for a clinical VT-stim protocol; (*b*) the simulated protocol for two extrastimuli, with coupling interval of 100 ms; (*c*) DT isochrones for S1 stimulus and (*d*) S2 stimulus; we have a unidirectional block created in the isthmus.

large cohorts of clinical data; thus, computational improvements are still to be done to streamline the model construction workflow and the generation of patient-specific simulations.

3. RADIOFREQUENCY ABLATION

Another major component of the increasing rate of CVDs is the rise in cardiac arrhythmias caused by structural disorders of the heart such as myocardial scarring following myocardial infarction, which in turn produces life-threatening arrhythmias such as ventricular tachycardia (VT). Additionally, the prevalence of atrial fibrillation (AF), which is more and more recognized as having a major impact on the patient's quality of life and prognosis, is related to age and roughly doubles with each advancing decade, from 0.5 per cent at age 50–59 years to almost 9 per cent at age 80–90 years.

The clinical understanding and treatment of these patients is complicated and includes a wide range of therapies, going from pharmaceutical to devices (pacemakers and implantable defibrillators) and interventions (surgical or radiofrequency ablation (RFA)). In a subgroup of patients with chronic and debilitating arrhythmias (such as AF), the use of RFA has shown to be an effective cure. However, RFA is expensive (more than €5000), minimal-invasive and involves a significant radiation exposure for the patient. Additionally, in many cases, the procedure has to be repeated a number of times, with some patients receiving little long-term benefits. With well over 4.5 million patients with AF in Europe, RFA is also having a major impact on rising healthcare costs. Similarly, VT is now commonly being treated with the insertion of intracardiac defibrillators. Thus, while as already discussed RFA is expensive, in this context it has the potential of being a better and cheaper alternative therapy here.

Biophysical models of the cardiac electrophysiology can provide a better understanding of the mechanisms leading to AF [28] and VT [29] by performing various *in silico* experiments. Our objective is to develop personalized anatomical and biophysical models in order to improve the planning and guidance of RFA therapies on patients suffering from AF and VT. Indeed, those patient-specific models can evaluate the impact of some RFA lines on the induction of AF and VT. By testing several ablation strategies, we plan to estimate their potential efficacy and thus provide additional guidance to the cardiologists. One important difficulty in this approach is to cope with the chaotic nature of AF and VT while biophysical models lead to deterministic results. A way to tackle this issue is to perform several simulations with varying biophysical parameters in order to estimate probabilities of inducing AF and VT.

For the personalization of those models, we use patient-specific data such as invasive intracardiac electrical recordings obtained at the time of RFA for AF and during electrophysiological studies for VT. Multi-channel ECG recording (64+ leads), so-called body surface potential mapping (BSPM), is also considered in this research as a non-invasive pre-operative electrophysiology imaging technique (ECG imaging, electrocardiographic imaging (ECGI)). This technique can complement intracardiac mappings but requires solving an inverse problem in order to estimate action potential data on the epicardium of the patient's heart. Furthermore, near-simultaneous MRI imaging provides cardiac geometry, tissue characteristics (gadolinium late-enhancement MRI for highlighting scars in the myocardium in VT patients and ablation patterns in AF patients) and heart motion (for VT).

Towards this goal, a realistic model of the anatomy and electrophysiology of the atria has been developed in order to simulate AF. First, we are using a volumetric voxel representation of the atria with a rule-based, spatially varying thickness of the atrium wall. Furthermore, the anisotropy effects owing to specialized atrial structures (Bachmann's bundle, crista terminalis and pectinate muscles) are taken into account. A semi-automatic

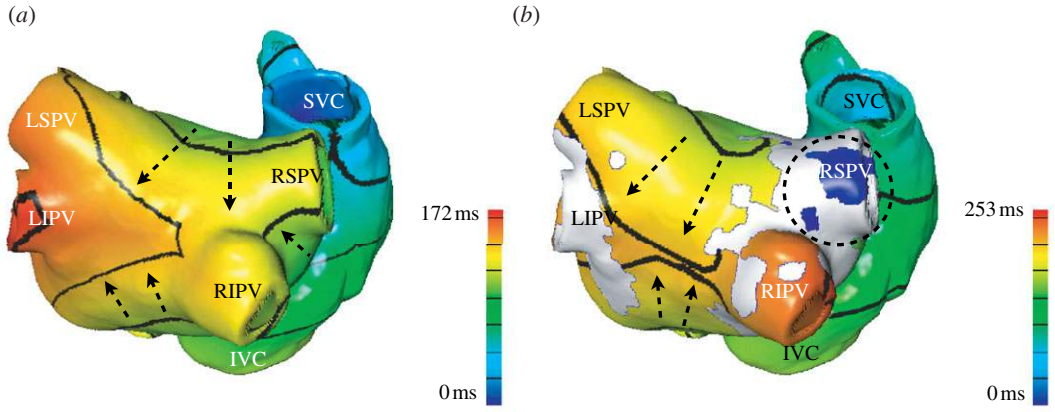

Figure 4. Local activation time maps resulting from electrophysiological simulations in a patient-specific bi-atrial model before (*a*) and after (*b*) ablation therapy. Damaged tissue (shown as white areas) was identified by late-enhancement MRI shortly after the procedure. Left atrial activation pattern is changed by the ablation lines (arrows). Right inferior pulmonary vein (RIPV) and left superior pulmonary vein (LSPV) were incompletely isolated from the left atrial myocardium and are thus activated both before and after the ablation. Right superior pulmonary vein (RSPV) was completely isolated and is thus not activated (right, circled blue area). Isochrones are shown as black lines. LIPV, left inferior pulmonary vein; SVC, superior vena cava; IVC, inferior vena cava.

procedure [30] has been devised to create patient-specific computational meshes of the atria, including some fibre orientation from patient's MR images [31]. Additionally, we are evaluating the influence of other interatrial conduction pathways on the development of atrial flutter and tachycardias.

The electrophysiology propagation is based on the Courtemanche–Ramirez–Nattel cell model [32] and adjusted to parameters provided in the literature. It also incorporates electrical remodelling owing to AF. Cell coupling is achieved by the monodomain formulation in a C++ framework [33]. The model shows good correspondence to measured action potentials of chronic AF patients. We are also working on the effect of haemodialysis (HD) on the atrial action potential and the increased prevalence for AF owing to HD [34]. Just as with the model for chronic AF, we aim to achieve with its consideration a personalization of the model to specific groups of patients.

Current work in progress includes the electrophysiological modelling of the atria after RFA by combining the joint effect of scar, ablated tissue and oedema. In particular, this study includes testing how the initiation of AF is affected by the addition of ablation lines. Long-term RFA success rates are moderate overall, perhaps owing to regenerating myocardium. Figure 4 shows an example of the impact of ablated tissue on excitation propagation during sinus rhythm in a patient-specific model. Damaged tissue from RFA was identified by late-enhancement MRI shortly after the procedure. Two pulmonary veins were not isolated during the procedure. The patient was re-admitted a few months after the intervention as AF recurred. Personalized electrophysiological models may be used to understand long-term RFA effects and thus increase success rates in the future.

For the simulation of post-infarcted VT, we are modelling the VT-stimulation (VT-stim) protocol used in clinics to induce VT. VT-stim is a clinical protocol that consists of a number of extrastimuli introduced at two ventricular sites (right ventricle (RV) apex and RV outflow tract), using various cycle lengths, with varying coupling intervals [35]. Induction of VT in this stimulation protocol may be due to both slow conduction and longer effective refractory period in the peri-infarct regions compared with healthy regions. The clinical VT-stim protocol has been simulated on a three-dimensional biventricular mesh built from patient images using a reduced electrophysiological model [36] discretized on a tetrahedral mesh with linear FEs. As reported by other research groups working on the induction of VT [29], it is important to account for the specificity of the pathological areas including the scars and peri-infarct zones in terms of boundary conditions. The anatomy and scar locations have been acquired and extracted from SSFP and late-enhancement MR images recorded at KCL. The cardiac fibre orientations are derived from an atlas generated from *ex vivo* canine hearts [37]. The peri-infarct region within scars corresponding to the isthmus plays a crucial role in VT induction. Indeed, the personalization of the electrophysiological model parameters from intracardiac non-contact mappings [38] leads to decreased conductivities in the isthmus compared with surrounding healthy tissues. Similarly, the personalized action potential duration (APD) restitution curves lead to longer APD in the isthmus compared with healthy tissue. In figure 3, VT-stim is simulated by pacing at RV-apex with 600 ms pacing cycle length and two extrastimuli with the shortest coupling interval of 100 ms. Stimulus S1 has a normal propagation in the isthmus; however, stimulus S2 faces a unidirectional block at the isthmus, which was created by APD heterogeneity and slow conduction of the previous S1 wave in the isthmus. This block creates a re-entry of the wave from the opposite direction, which is sustained and has a constant frequency. Thus, the induced re-entry is called as sustained monomorphic VT. More details about this work can be found in Relan *et al.* [38]. Current limitations of this work include the

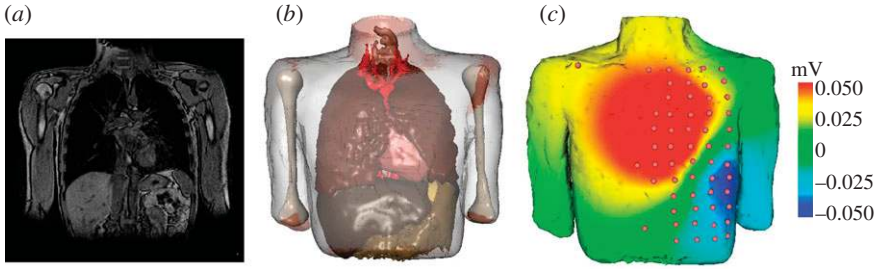

Figure 5. Segmentation of a volunteer dataset. (*a*) MRI slice from the thorax; (*b*) three-dimensional visualization of the segmented thorax; (*c*) interpolation of BSPM onto the thorax mesh.

uncertainty in the image segmentation of scars and peri-infarct zones as well as their characterization in terms of electrophysiological properties. Furthermore, the non-deterministic nature of VT should be assessed as well as the difference of VT-stim predictions between *in silico* experiments and electrical mappings measured on the patient.

A protocol for the acquisition of ECGI at St Thomas' Hospital has been established based on an 80-channel vest of electrodes coupled with whole-heart and thorax MRIs. This has led to the acquisition of four datasets on healthy volunteers and patients with paroxysmal AF. Endocardial data acquisition is available for one of those patients as a way to evaluate the accuracy of activation time reconstruction. The analysis of those datasets requires performing several image- and signal-processing steps [31,39]. These include the whole-heart MRI segmentation for the endocardium of the ventricles and atria and epicardium of the left ventricles (LVs). The epicardial walls of the left and right atria and right ventricle are manually segmented. Another tedious task includes the manual segmentation of several inner organs from MRI. Finally, the continuous ECGI data are converted into an averaged and filtered template ECGI signal and interpolated onto the segmented MRI thorax (figure 5).

Based on the segmented dataset and taking into account the non-homogeneous electrical conductivities of the thorax, the propagation of the extracellular potential from the atria to the body surface has been simulated. First, a comparison between the measured BSPM and the simulated potential has been performed [31]. In particular, we have performed a thorough sensitivity analysis of the effect of conduction velocity, initial stimulation points and mesh size on the simulated P-wave signal. Second, the inverse problem of electrocardiography has been addressed, i.e. estimating the times of activation on the atria given the measured BSPM. For calibration purposes, simulated BSPM corrupted with noise has been tested as an input of the inverse mapping and activation times on the atria have been estimated using Tikhonov regularization [40]. Along with the generalized minimal residual method, Tikhonov regularization is used by the leading groups in the field [41]. Additional *a priori* knowledge on the activation patterns has been used to further constrain the solution, including several new methods that are based on assumed action potential curves and the effects of local depolarizations on the BSPM. Our future work will focus on improving the stability of the methods and on a comprehensive approach to reduce the effects and sources of modelling errors.

4. LEFT VENTRICULAR ASSIST DEVICE IMPLANTATION AND CONGENITAL TRANSPOSITION

Building on the electromechanical work outlined above provides the opportunity to include the addition of fluid mechanics in the cardiac modelling frameworks and address the loss of myocardial contractility in HF. The resultant reduction in the ability of the heart to pump blood in this disease currently accounts for a significant reduction in both mortality and morbidity in Western society. Despite this significance, the aetiology of the disease remains poorly understood, is complex and context-specific, spanning age groups and conditions. In young adults who have undergone surgery to correct congenital transposition (where the two main arteries leaving the heart are reversed at birth), the initially successful switch of the ventricles often ultimately results in the systemic ventricle, now on the right of the heart, failing. Such developments bring into focus the appropriateness of the initial surgical intervention and how subject groups are assessed and selected for procedures.

In elderly populations, HF is rapidly becoming an epidemic, a fact confounded by the severe lack of donor hearts, with transplant as the only established long-term solution. To create a bridge to transplant, LVADs are often surgically inserted by reducing load by pumping blood from the bottom of the LV directly into the aorta. In a recent and highly promising development, a small but significant (approx. 5%) subpopulation with implanted LVADs (Berlin Heart, Steglitz, Germany) has completely recovered, undergoing cardiac remodelling to the point where the LVAD can be removed. The mechanisms underlying such remodelling remain conjecture; however, if the underlying mechanisms were properly understood, customizing LVAD function via patient-specific tuning to both investigate how LVAD placement and flow rate could be optimized to benefit cardiac function and promote remodelling now has the potential to provide a huge clinical gain.

While the treatment developments outlined above are encouraging, solutions that identify the interventions to produce individual benefits in congenital and LVAD patients require input from multiple disciplines.

Using multi-modal data, our goal is to exploit the potential of multi-scale computational frameworks to interpret unique clinical imaging to optimize clinical protocols and direct device design and tuning work. This research is motivated by the clinical outcomes of developing tools to specifically (i) redefine the criteria for patient selection to define the most appropriate target group for surgical intervention, (ii) tune the performance of an LVAD to optimize the haemodynamic benefits to a specific individual, and (iii) identify the common ventricular flow-myocardial wall mechanic features that promote remodelling of the ventricle and recovery from HF.

Our approach is to refine our existing modelling framework to develop an integrated computational model of cardiac contraction coupled to ventricular fluid dynamics [42]. Full nonlinear passive and active constitutive relations are combined with the finite deformation governing equations using the FE method. Using the coupling approach for general fluid solid modelling previously developed by Nordsletten *et al.* [43–45], the biophysics governing the myocardial deformation (solid mechanics) has been coupled to fluid mechanics within the ventricular chamber. The resulting equations have been solved by an FE-based arbitrary Lagrange Eulerian (ALE) approach. The endo- and epicardial meshes were fitted to the data using a nonlinear fitting process, performed using the CMISS software package.[7] The volume meshes were constructed by linear interpolation between the corresponding nodes on the endo- and epicardial surfaces. To ensure smoothness of flow, inflow and outflow cannulae were constructed at the mitral and aortic valve planes. The LVAD cannula geometry was provided by the device manufacturer (Berlin Heart, Steglitz, Germany). The fluid mesh, within the LV, was constructed using Cubit[8] and the fluid–solid interface elements were defined as a separate domain. Simulations are run on these fitted geometries in order to capture the effect LVADs have on ventricular function and blood recirculation within the LV cavity. Results from one of these simulations are shown in figure 6, where mean inflow velocity was prescribed so that filling was isovolumetric over one cardiac cycle and inflow and outflow velocities fitted from comprehensive MR measurements. Boundary conditions for the mechanics problem were included to fix both the mitral valve plane and the apex, where the LVAD cannula was attached.

These simulations reveal the complex dynamics that occur around the LVAD cannula, which in turn result in recirculation at the apex, below the LVAD mouth. Also of note is the absence of a primary vortex typical of normal ventricular filling owing to the presence of the LVAD cannula. Furthermore, the action of the LVAD cannula close to the myocardial wall has the potential to induce suction effects on the endocardium, producing a significant impact of cardiac pump function. Balancing the impact of an LVAD on ventricular flow with this negative impact of suction presents an optimization problem whereby pump function, currently set at a constant velocity in axial flow LVADs, could be tuned to optimize the mechanics of the cardiac cycle. Current work is focused on validation of the model using comprehensive data-acquired preimplantation and CT imaging after the pump has been implanted. From this validated framework, the model will be applied to explore the functional envelope induced by different LVAD flow profiles as part of the focus of our ongoing work.

In young adults, we focus on hypo-plastic left heart, which is a condition that affects four to five children out of 10 000 births and poses a serious threat to life, requiring immediate surgical treatment in the majority of the cases. Hypo-plastic left heart patients can rely solely on the right ventricle as a motor for the systemic and the pulmonary circulation, the left one being atrophied or underdeveloped. To assist the surgeon in planning the intervention, we use biophysical simulations to assess diastolic dysfunction through the analysis of pressure gradients and myocardial relaxation (figure 7). In the rapid filling phase (early diastole), the annular velocity during the ventricle elongation, e', is recorded as well as the velocity of the inflow at the inlet valve, E. Previous studies in the literature have demonstrated that the ratio E/e' is an important clinical parameter to predict the filling pressures and to highlight diastolic abnormalities. The flow propagation and vortex formation mechanism is analysed in the hypo-plastic left heart cases and compared with the previous results obtained from patients affected by congenitally corrected transposition of the great arteries. Our goal in this work is to use the information provided by the model to underpin a clinical trial at the end of the project to test the value of computational metrics for selecting patients who will respond to surgical treatment.

5. CORONARY PERFUSION

CAD is the major cause of mortality worldwide, despite the fact that currently available strategies to lower individual risk factors and treat evident coronary artery stenoses have reduced cardiovascular event rates by 20–30%. In addition, a definite exclusion of epicardial coronary artery stenosis is mainly achieved by invasive angiography. Owing to the high risk of the disease and the difficulty in excluding it, a large number of patients undergo invasive stenosis treatment with negative results. Therefore, developing improved modalities for the diagnosis and treatment of coronary disease is important for both increased quality of life and reduction of the cost associated with CAD. The ability to assess in a personalized manner epicardial CAD as well as disturbed blood flow control and increased microvascular resistance earlier and with higher accuracy will allow us to improve prevention and reduce health costs. Assessing alterations of coronary or microvascular flow is also important in patients with other cardiac abnormalities including aortic stenoses and HF, which are disease foci discussed elsewhere in this paper.

[7] http://www.cmiss.org
[8] http://cubit.sandia.gov

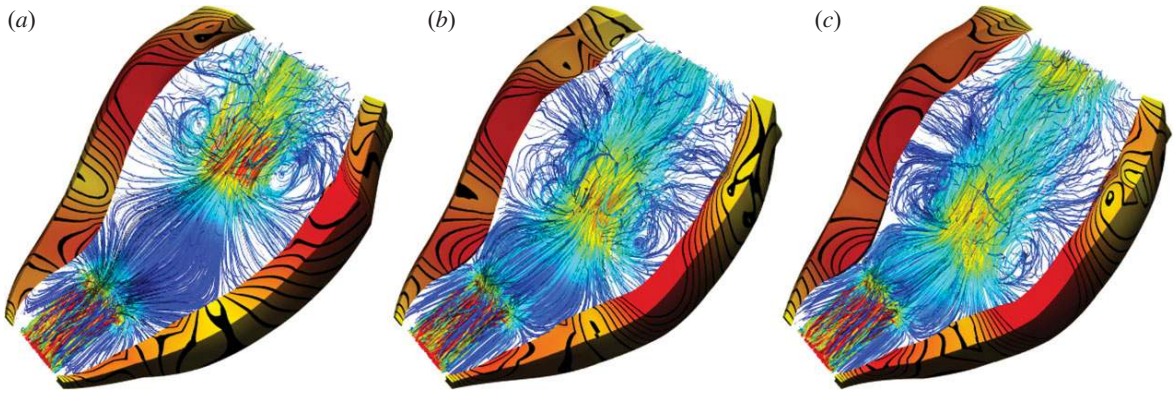

Figure 6. Diastolic filling under LVAD support. Simulation was run with sinusoidal mitral valve inlet velocity to replicate reduced pulse intensity under LVAD support. (*a*) Peak inflow velocity, 0.09 m s^{-1}, (*b*) minimum inflow velocity, 0.04 m s^{-1}, (*c*) secondary inflow peak forming, 0.065 m s^{-1}. LVAD cannula outflow velocity was 0.22 m s^{-1} throughout the simulation. Streamlines show flow patterns in the LV cavity, blue representing low and red high flow velocities. On the myocardial wall, yellow represents low and red high deformation, and black lines are contour bands. Note the uniaxial flow from the inlet valve to the outflow cannula and the absence of a primary vortex. Vortices form either side of the peak velocity jet, travelling apex to base, which cause outward deformation of the wall normal to the jet path. Also note the suction effects on the LV wall close to the cannula mouth. Recirculations are not apparent at the apex below the cannula mouth.

In the past, the focus has been on the improvement of measurement of characteristic dimensions of coronary stenosis in order to predict its clinical significance. However, this clinical significance is determined by the limiting effect a stenosis has on the myocardial perfusion increase needed for exercise levels above basal daily activity. Specifically, coronary flow reserve [46] is defined as the ratio between maximal reachable coronary flow and maximal obtainable flow at exercise and hence requires the measurement of flow under two conditions, while one may argue that only the limitations on maximal obtainable perfusion are relevant. Based on a number of assumptions, the reduction in maximal flow can be derived from the relative pressure drop over a coronary stenosis during pharmacological-induced maximal vasodilation, which is denoted as fractional flow reserve [47,48]. It has become clear that these physiological indices are doing better in predicting the need for stenosis treatment than angiography alone [6,49]. However, different indices may result in different treatment suggestions, indicating that a more precise analysis of coronary (patho) physiology is needed [50], which has become possible by the introduction of a guide wire measuring distal pressure and flow velocity simultaneously [51].

Earlier physiological studies have clearly demonstrated that the inner layer of the heart muscle, the subendocardium, is more vulnerable to ischaemia than the outer layers of the heart [52]. Only recently techniques have become available to measure the distribution of blood perfusion over the heart muscle clinically [53]. In particular, MRI-based methods are promising because of their practical clinical application and high resolution [54]. MRI basically measures arrival and passage of a contrast agent through the tissue. However, interpretation of these image-based methods requires more detailed understanding of transport of blood through the microcirculation.

In the past, several efforts have been made to model coronary flow distribution [55–57] based on assumed branching rules of coronary arteries, which are based on certain space-filling criteria or branching rules derived from coronary corrosion casts [58]. Our goal is to deliver a multi-scale, multi-physics model to allow a much more sensitive and precise sensing of perfusion abnormalities of cardiac tissue not only in the epicardial arteries but also in the mircocirculation. The approach is to develop such a model based on the real measured anatomy of the coronary vascular bed down to the micron diameter level, its interrelationship with heart muscle fibre orientation and the biophysical processes responsible for the compression of intramural vessels, especially in the subendocardium [7,59,60]. Similar approaches have been proposed before and indeed have contributed substantially to our present insights. In the absence of information, three-dimensional vascular branching models have been constructed [55,56] based on stochastic branching rules derived from corrosion casts of pig coronary vasculature [58]. Simplified distribution models indicate that the interaction between layers at different myocardial depths depends on epicardial stenosis resistance [61]. The fibre orientation has been precisely measured in small hearts and successively applied to the large heart models [62]. The innovation of the model constructed within the euHeart project is within the application of realistic three-dimensional information on vascular branching and fibre sheet information as obtained by a novel imaging cryomicrotome [63] integrated into personalized mechanical models of heart contraction [26]. In this model, perfusion in the microcirculation is implemented using FE-based porous elastic techniques to couple perfusion (modelled using Darcy flow) to contracting tissue (modelled via large deformation mechanics). Pressure boundary conditions are applied to the endocardium along with no-flux flow conditions at the endo- and epicardial surfaces. Apart from its clinical use in diagnosis support, the resulting model provides potential to analyse a wider variety of biophysical processes relevant at different levels in the coronary circulation as recently reviewed [62,64].

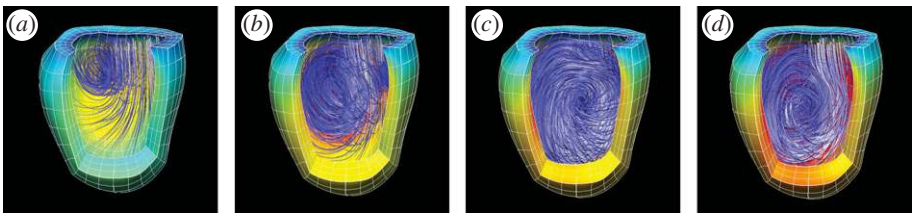

Figure 7. The vortex formation in the systemic right ventricle of a patient with hypo-plastic left heart. The ring vortex is formed during the peak E wave in proximity of the aortic valve, as shown in figure 1*a*. During the deceleration period, it expands and travels axially away from the formation region (figure 1*b*). At diastasis (figure 1*c*), the maximum volume expansion is attained on a circumferential plane located just below the valve orifices and the two vortices merge into one complex swirling structure. No additional vortex pair is observed during the atrial contraction (figure 1*d*), unlike in the normal LV filling, where a weak ring vortex appears near to the mitral inlet.

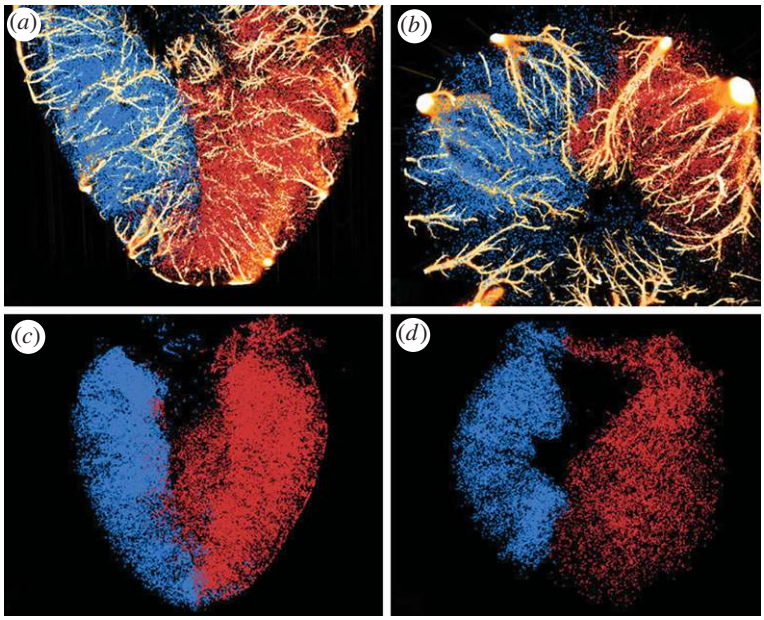

Figure 8. Separation of microsphere colours, shown as three-dimensional microsphere distributions for a 10 mm thick slab in the (*a*,*c*) sagittal and (*b*,*d*) transverse plane of two canine hearts. (*a*,*b*) Yellow microspheres injected into the LCX and red microspheres into the left anterior descending coronary artery (LAD), together with detected fluorescent casting material. (*c*,*d*) Carmine microspheres injected into the LCX and scarlet microspheres into the LAD. A clear separation of perfusion territories can be seen for both hearts. (From van Horssen *et al.* [61], with permission of the journal and author).

In the past 2 years, the focus has been on improving technologies for obtaining and interpreting images [65,66]. Based on the point spread function, the images are filtered, followed by segmentation of the vascular structure, which now will allow for computation of flow distribution over the vascular tree into the different compartments of the myocardium. These models will have to be validated by clinical image-based perfusion studies as well as animal studies [67] for which microsphere distribution provides a gold standard (figure 8). The imaging of the intramural vasculature in post-mortem human hearts will be used to increase our insights into specific vascular abnormalities such as end-stage HF [68].

From the clinical side, studies are under way to compare MRI perfusion measurements with epicardial artery-derived indices for inducible ischaemia. Specifically, wave intensity analysis (WIA) has been introduced for coronary arterial flow analysis [69]. WIA combines the time derivatives of coronary pressure and velocity signals. Since flow velocity and pressure pulsatilities are generated by compression of the microcirculation, WIA allows us to derive parameters describing microvascular function and in future work will be used to validate the model under development [70–72].

The challenge in applying the model analysis to clinical data is the integration of perfusion distribution data by MRI and selective haemodynamic measurements in epicardial arteries by smart guide wires used for catheterization. Mechanistically, these phenomena are related since the contraction of the heart is responsible for perfusion distribution by impeding microvascular flow at the local level and the pulsatile nature of coronary flow and pressure in the epicardial arteries. However, it is not clear yet whether the sensitivities of the interactions are similar at similar level of coronary disease. It is conceivable that the epicardial haemodynamic alterations are early signs of vascular disease while perfusion disturbances only occur after some

larger progression of disease. For these distinctions, clinical validation of the model under development is needed.

6. AORTIC COARCTATION

Aortic coarctation is a constriction in the aorta, usually located just after the branching of the arteries that supply the head and arms. It is one of the most common congenital heart defects, affecting one in 10 000 individuals. A significant proportion (10–20%), treated in the neonatal period, develop re-coarctation [73].

The fundamental problem associated with aortic coarctation is that it increases the after-load on the heart, reducing flow for a given amount of work and increasing cardiac and arterial pressures proximal to the coarctation, including in the vessels that supply the head [74]. This increase in after-load leads to increased risk of CAD and stroke.

In principle, aortic coarctation is a physics problem that is a perfect subject for study using the techniques of computational fluid dynamics. The easiest coarctations to detect are those that feature a significant geometrical narrowing of the vessel, visible in diagnostic images. Such coarctations produce a pressure elevation that is, at least as a first approximation, computable from the Bernoulli equation, although the fact that the flow is pulsatile, combined with often complex anatomy, might indicate a requirement for more sophisticated computational fluid dynamics (CFD) computations using three-dimensional models constructed from the medical images. More subtle coarctations might present little, or even no, significant narrowing but are characterized by an increased local stiffness of the vessel. The aorta is essentially an elastic tube, the physics of which can be approximated by a one-dimensional model, and a local stiffness change causes wave reflections that again lead to elevated cardiac and proximal vessel pressures. A brief review of computational methods applied to aortic coarctation is presented by Ladisa *et al.* [75].

In clinical practice, pressure drops are measured invasively using a pressure catheter, usually under a protocol that includes a pull-back through the region of the stenosis. A complicating factor is that there are large numbers of patients with mild coarctation or re-coarctation who have little pressure gradient at rest, but hypertension particularly on exercise. Often, but not always, this condition can be simulated pharmacologically and pressure drops can again be measured invasively. Our first target of the analysis of aortic coarctation is to explore in what percentage of case the pressure drop might be predicted reliably from the description of the geometry alone (i.e. without any information on local or global stiffnesses). This includes the extrapolation from the rest to the stress condition. There is strong clinical interest in the identification, without invasive measurements, of those coarctations that will become physiologically significant under exercise.

euHeart has built a processing chain and a workflow, suitable for operation in a clinical environment, that take a medical image of the aorta, together currently with measured transient flows and pressures as inputs and computes the pressure drop across the coarctation. Flow is computed by the integration of through-plane MRI velocity measurements on a cross section in the ascending aorta and in cross sections in the branching vessels at the top of the arch, and applied to the model as a boundary condition at these locations. Invasive pressure catheter measurements are applied at the distal end of the model, in the descending aorta. The CFD solution is computed in ANSYS CFX, a commercial code that uses an element-based finite-volume method with second-order discretization in space and time. Refinements to the workflow include the use of zero-dimensional models to compute boundary conditions, possibly tuned to individual patient measurements. A range of solver options is possible, from the simplest rigid-walled analysis through to full-system fluid–solid interaction solutions of the type described by Kim *et al.* [76].

Preliminary results have been produced for a series of five cases, each under boundary conditions representative of rest and pharmacological stress conditions, using a transient, rigid-walled analysis, with the pressure drop computed at the instant of peak flow. Figure 8*a*,*b* illustrate the computed distribution of pressure in the aorta (spatial distribution on the inner surface of the artery at peak flow and temporal distribution along the centreline, respectively) for one coarctation case. Figure 9*c* illustrates the simulation of a pressure catheter pull-back, overlaid on the clinical data for this operation. Although the Bernoulli pressure well in the throat of the coarctation is deeper in the simulation than in the clinical measurement, the pressure drop across the coarctation is well represented even with this simple analysis model.

In all cases, as would be expected, the simulation (using measured flow boundary conditions) predicted an increase in the pressure drop under stress relative to that under the rest condition. In four of the five cases, the analysis provided a prediction of the pressure drop under rest conditions that was within the range of clinical measurements (with an error of 3 mmHg or less) and certainly of sufficient accuracy for diagnostic purposes. As a check, additional analyses were performed on subjects with normal aortas and, again as expected, the pressure drops were very low (of the order of 1 mmHg). The extrapolation to the stress condition proved less reliable, with errors of the order of 30 per cent relative to the measured pressure drop, but nevertheless in four of the cases, the analysis correctly predicted that physiologically significant pressure gradients (greater than 40 mmHg) were present. Although improvements of the processing chain are underway, the results already indicate that clinically meaningful computations of the physiological severity of the coarctation should be possible. The most serious simplification in the analysis method for which results are presented in this section is the assumption of rigid walls of the aorta, which means that capacitive and wave transmission effects are not captured, but further (R. Hose & I. Valverde 2011, unpublished data) results indicate that this does not have a strong influence on the computed pressure drops. The use of measured

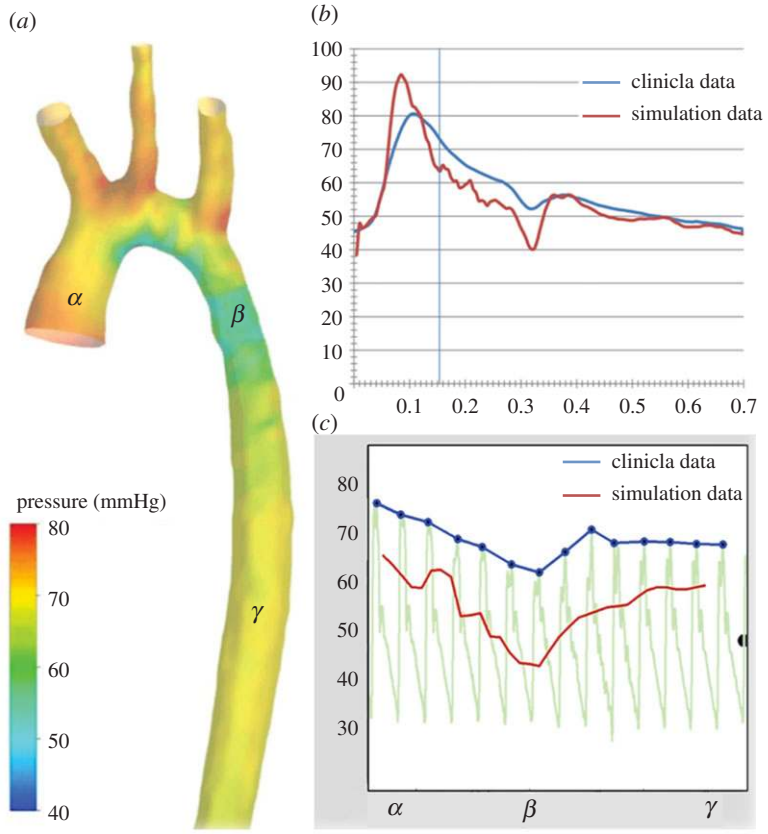

Figure 9. Measured and computed pressures in aorta for one coarctation case: (*a*) computed distribution of pressure on internal surface at peak flow, (*b*) measured and computed pressure versus time on the centreline over one cardiac cycle, and (*c*) measured and computed catheter pullback.

flow boundary conditions on the smaller branching vessels at the top of the arch is a further restriction, and indeed a likely source of error and inconsistency, and there is a strong case for the adoption of tuned Windkessel models as an alternative.

7. DISCUSSION AND CONCLUSIONS

In this article, we have aimed to summarize the ongoing work within the euHeart project to develop and apply patient-specific models within a number of specific contexts. Given the wide context of this work, these summaries are necessarily brief and the interested reader is referred to the detailed literature in each of the specific areas. However, a number of general conclusions can be drawn.

While the development of multi-scale, multi-physics models, such as the cardiac frameworks demonstrated above, continues to progress, the clinical diagnosis and treatment of CVD still largely depends on complex mental integration based on specific clinical experience and phenomenological-derived indexes. In addition to improved patient selection and therapy optimization, the application of these models also allows the concept of 'intelligent' imaging to be introduced. Specifically, this requires a transition towards quantified metrics that are mechanistically linked to cardiac function to enable two interrelated issues to be addressed; specifically (i) how can imaging protocols be optimized in specific clinical contexts to improve diagnosis and treatment planning and (ii) what is the information content that can be extracted from the clinical data which will most effectively inform clinical practice. The integration of state-of-the-art imaging modalities, functional measurements and cardiac models now provides exactly the required foundation from which to progress this goal further.

The types of numerical methods that are used in the euHeart programme (FEs, finite differences, etc.) have long been employed in other industries, including aerospace and automotive applications. It is recognized that there is a strong need for benchmarks against which codes can be validated. These are developed and promoted by agencies like the National Agency for Finite Element Methods and Standards in the UK. The computations performed in euHeart cover a broad spectrum of physics (reaction–diffusion, electromechanical and fluid mechanics) over a wide range of complexity (up to state-of-the-art fully coupled multi-physics simulations). In order to achieve credibility, it is important that our simulation tools and workflows are validated. Recently, the FDA has published [77] a CFD benchmark to challenge the community to produce accurate simulations of the flow in a very simple geometry but under challenging Reynold's numbers. Some of our partners have experience in organizing cross-institutional challenges in the cardiovascular domain to the stimulate benchmarking and best practices across groups [78]. The long-term goal is to demonstrate to the FDA whether simulation can provide a credible

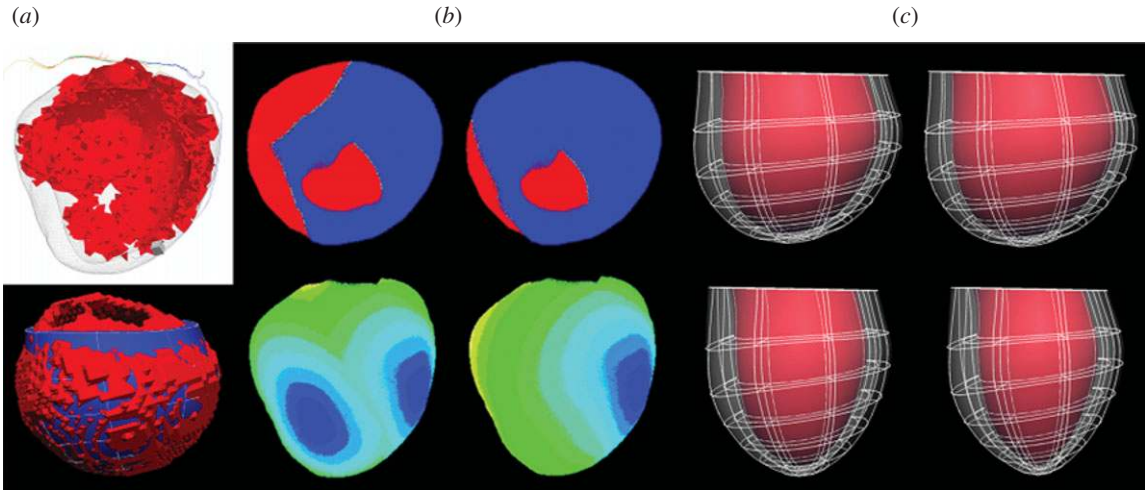

Figure 10. Patient-specific simulation results in a CRT case. (*a*) Patient-specific FE meshes (tetrahedral mesh at the top, showing the scar and the centreline of the coronary tree in three dimensions; hexahedral mesh at the bottom). (*b*) Electrophysiological simulation results obtained with the tetrahedral mesh with two leads (left) and with one lead (right) (propagation wave at the top and local activation map at the bottom). (*c*) Mechanical simulation results obtained with the hexahedral mesh (four different time points, from diastole to systole).

method of assessment of devices like LVADs. Such developments would have a potential impact on a much quicker identification of good-performance devices, discarding inadequate device concepts or designs, and the concomitant safety and savings in time and cost associated with early identification of unsuccessful devices. euHeart has recognized the importance of carefully validated benchmarks as a community resource against which the performance of numerical codes can be evaluated, and has made a series of test problems and results publicly available through its euHeartDB database [9]. Already this has proved valuable in comparing results from wider community members, outside the euHeart programme, including the identification of discrepancies that have led to code improvements.

The euHeart project focuses on the translational aspects of multi-scale cardiovascular modelling into clinical environments and the demonstration of potential clinical benefits on patient outcome. Several workflows are being developed jointly between scientists and clinicians. One of the most advanced of them is the one focused on CRT presented above, covering the whole chain from access to clinical data and their processing, patient-specific modelling, simulation and treatment planning. For this reason, one multi-centre pilot trial, including approximately multi-modal data for 120 patients acquired in three clinical centres in three different countries (UK, France and Spain), will be performed. The main goal of this pilot trial is to demonstrate the clinical benefit in determining the optimal lead placement and pacing sequence in CRT by prospectively analysing with the developed tools the patient database. The pilot trial is currently in the phase of data acquisition and preliminary testing of the developed imaging and modelling algorithms on these patient-specific data, as shown in figures 4 and 10. The image and model processing of the whole database of patients remains a challenge that will be faced during the second part of the project. The clear definition of the different workflows as well as the integration of the different tools into a common software platform will hopefully help on this issue. Finally, it must be pointed out that this pilot trial is a first initiative towards a large-scale clinical trial including modelling tools, but further joint discussions between clinicians and technicians are still needed to effectively embed these advanced tools into typical clinical trials.

The longer term outcome of the euHeart programme will be a consistent, biophysically based framework for quantitative data integration, interpretation of information and knowledge extraction using the developed computational imaging and modelling tools. Our hope and expectation is that this in turn will support a paradigm shift away from clinical indices determining treatment options based on population-based patient selection or risk profiles and a move towards true personalization of care based on the interpretation of the patient data and history in the context of his/her specific physiology. Our goal and expectation for this work, perhaps echoed across the VPH community, is that through this project we will be able to collectively make a significant positive impact on the treatment and prevention of heart disease.

This work was supported by the European Commission (FP7-ICT-224485:euHeart) and the authors would like to acknowledge the work of the whole euHeart consortium.

REFERENCES

1 Leal, J., Luengo-Fernández, R., Gray, A., Petersen, S. & Rayner, M. 2006 Economic burden of cardiovascular diseases in the enlarged European Union. *Eur. Heart J.* **27**, 1610–1619. (doi:10.1093/eurheartj/ehi733)

2 Uribe, S., Muthurangu, V., Boubertakh, R., Schaeffter, T., Razavi, R., Hill, D. L. & Hansen, M. S. 2007 Whole-heart cine MRI using real-time respiratory self-gating. *Magn. Reson. Med.* **57**, 606–613. (doi:10.1002/mrm.21156)

3 Kilner, P. J., Yang, G. Z., Wilkes, A. J., Mohiaddin, R. H., Firmin, D. N. & Yacoub, M. H. 2000 Asymmetric

redirection of flow through the heart. *Nature* **404**, 759–761. (doi:10.1038/35008075)
4 Gebker, R., Schwitter, J., Fleck, E. & Nagel, E. 2007 How we perform myocardial perfusion with cardiovascular magnetic resonance. *J. Cardiovasc. Magn. Reson.* **9**, 539–547. (doi:10.1080/10976640600897286)
5 Lefebvre, C. & Hoekstra, J. 2007 Early detection and diagnosis of acute myocardial infarction: the potential for improved care with next-generation, user-friendly electrocardiographic body surface mapping. *J. Am. J. Emerg. Med.* **25**, 1063–1072. (doi:10.1016/j.ajem.2007.06.011)
6 Tonino, P. A. *et al.* FAME Study Investigators. 2009 Fractional flow reserve versls angiography for guiding percutaneous coronary intervention. *N. Engl. J. Med.* **360**, 213–224.
7 Lee, J., Niederer, S., Nordsletten, D., Le Grice, I., Smaill, B., Kay, D. & Smith, N. 2009 Coupling contraction, excitation, ventricular and coronary blood flow across scale and physics in the heart. *Phil. Trans. R. Soc. A* **367**, 2311–2313. (doi:10.1098/rsta.2008.0311)
8 Niederer, S. A., Fink, M., Noble, D. & Smith, N. P. 2009 A meta analysis of the physiome paradigm with application to cardiac electrophysiology. *Exp. Physiol.* **94**, 486–495. (doi:10.1113/expphysiol.2008.044610)
9 Gianni, D., McKeever, S., Britten, R., Yu, T., Hunter, P. J., Delingette, H., Frangi, A. F. & Smith, N. P. 2010 A step towards the implementation of the virtual physiological human project: sharing and reusing geometrical models of the heart over the Web. *Phil. Trans. R. Soc. A* **368**, 3039–3056. (doi:10.1098/rsta.2010.0025)
10 Ecabert, O. & Smith, N. P. 2008 euHeart: integrated cardiac care using patient-specific cardiovascular modeling, *Biomedical Optics & Medical Imaging 2008 SPIE.* (doi:10.1117/2.1200804.1126)
11 Larrabide, I. *et al.* 2009. GIMIAS: an open source framework for efficient development of research tools and clinical prototypes. *FIMH'09*, LNCS 5528, pp. 417–426. Berlin, Germany: Springer.
12 Smith, N. P., Nickerson, D., Crampin, E. J. & Hunter, P. J. 2004 Computational modelling of the heart. *Acta Numer.* **13**, 371–431. (doi:10.1017/S0962492904000200)
13 Strickberger, S. A., Conti, J., Daoud, E. G., Havranek, E., Mehra, M. R., Piña, L. L. & Young, J. 2005 Patient selection for cardiac resynchronization therapy. *Circulation* **111**, 2146–2150. (doi:10.1161/01.CIR.0000161276.09685.4A)
14 Dickstein, K. *et al.* 2010 Focused update of ESC guidelines on device therapy in heart failure: an update of the 2008 ESC guidelines for the diagnosis and treatment of acute and chronic heart failure and the 2007 ESC guidelines for cardiac and resynchronization therapy. Developed with the special contribution of the Heart Failure Association and the European Heart Rhythm Association. *Eur. Heart J.* **31**, 2677–2687. (doi:10.1093/eurheartj/ehq027)
15 van Deursen, C., van Geldorp, I. E., Rademakers, L. M., van Hunnik, A., Kuiper, M., Klersy, C., Auricchio, A. & Prinzen, F. W. 2009 Left ventricular endocardial pacing improves resynchronization therapy in canine left bundle-branch hearts. *Circ. Arrhythm. Electrophysiol.* **2**, 580–587. (doi:10.1161/CIRCEP.108.846022)
16 Auricchio, A. & Prinzen, F. W. 2011 Non-responders to cardiac resynchronization therapy. *Circ. J* **75**, 521–527.
17 Duckett, S. G., Ginks, M., Knowles, B. R., Chiribiri, A., Ma, Y. L., Razavi, R., Schaeffter, T., Carr-White, G., Rinaldi, C. A. & Rhode, K. 2010 A novel cardiac MRI protocol to guide successful cardiac resynchronization therapy implantation. *Circ. Heart Fail* **3**, e18–e21 (doi:10.1161/CIRCHEARTFAILURE.110.936328)
18 Young, A. A. & Frangi, A. F. 2009 Computational cardiac atlases: from patient to population and back. *Exp. Physiol.* **94**, 578–579. (doi:10.1113/expphysiol.2008.044081)
19 Peters, J., Ecabert, O., Meyer, C., Kneser, R. & Weese, J. 2010 Optimizing boundary detection via simulated search with applications to multi-modal heart segmentation. *Med. Image Anal.* **14**, 70–84. (doi:10.1016/j.media.2009.10.004)
20 Lehmann, H., Kneser, R., Neizel, M., Peters, J., Ecabert, O., Kühl, H., Kelm, M. & Wesse, J. 2009. Integrating viability information into a cardiac model for interventional guidance. *FIMH'09*, LNCS 5528, pp. 312–320. Berlin, Germany: Springer.
21 Velut, J., Toumoulin, C. & Coatrieux, J.-L. 3D coronary structure tracking algorithm with regularization and multiple hypotheses in MRI. In *2010 IEEE Int. Symp. on Biomedical Imaging: From Nano to Macro, April 2010*, pp. 37–40.
22 De Craene, M. *et al.* 2010 Temporal diffeomorphic free-form deformation for strain quantification in 3D-US images. *MICCAI'10*, LNCS 6362, pp. 1–8. Berlin, Germany: Springer.
23 Parsai, C. *et al.* 2009 Toward understanding response to cardiac resynchronization therapy: left ventricular dyssynchrony is only one of multiple mechanisms. *Eur. Heart J.* **30**, 940–949. (doi:10.1093/eurheartj/ehn481)
24 Duchateau, N., De Craene, M., Piella, G., Silva, E., Doltra, A., Sitges, M., Bijnens, B. H. & Frangi, A. F. 2011 A spatiotemporal statistical atlas of motion for the quantification of abnormal myocardial tissue velocities. *Med. Image. Anal.* **15**, 316–328. (doi:10.1016/j.media.2010.12.006)
25 Camara, O. *et al.* 2009 Cardiac motion estimation from intracardiac electrical mapping data: identifying a septal flash in heart failure, *FIMH'09*, LNCS, 5528, pp. 21–29. Berlin, Germany: Springer.
26 Lamata, P., Niederer, S., Barber, D., Norsletten, D., Lee, J., Hose, R. & Smith, N. 2010 Personalization of cubic Hermite meshes for efficient biomechanical simulations. *Med. Image. Comput. Comput. Assist Interv.* **13**, 380–387.
27 Romero, D., Sebastian, R., Bijnens, B. H., Zimmerman, V., Boyle, P. M., Vigmond, E. J. & Frangi, A. F. 2010 Effects of the Purkinje system and cardiac geometry on biventricular pacing: a model study. *Ann. Biomed. Eng.* **38**, 1388–1398. (doi:10.1007/s10439-010-9926-4)
28 Jacquemet, V., Kappenberger, L. & Henriquez, C. S. 2008 Modeling atrial arrhythmias: impact on clinical diagnosis and therapies. *IEEE Rev. Biomed. Eng.* **1**, 94–114. (doi:10.1109/RBME.2008.2008242)
29 Vigmond, E., Vadakkumpadan, F., Gurev, V., Arevalo, H., Deo, M., Plank, G. & Trayanova, N. 2009 Towards predictive modelling of the electrophysiology of the heart. *Exp. Physiol.* **94**, 563–577. (doi:10.1113/expphysiol.2008.044073)
30 Krueger, M. W., Weber, F. M., Seemann, G. & Dössel, O. 2009 Semi-automatic segmentation of sinus node, Bachmann's bundle and terminal crest for patient specific atrial models. World Congress on Medical Physics and Biomedical Engineering. *IFMBE Proc.* **25/4**, 673–676. (doi:10.1007/978-3-642-03882-2_180)
31 Krueger, M. W., Rhode, K., Weber, F. M., Keller, D. U. J., Caulfield, D., Seemann, G., Knowles, B. R., Razavi, R. & Dössel, O. 2010 Patient-specific volumetric atrial models with electrophysiological components: a comparison of simulations and measurements. *Biomed. Techn./Biomed. Eng.* **55**, 54–57.
32 Courtemanche, M., Ramirez, R. J. & Nattel, S. 1998 Ionic mechanisms underlying human atrial action potential properties: insights from a mathematical model. *Am. J. Physiol.* **275**, H301–H321.

33 Seemann, G., Sachse, F. B., Karl, M., Weiss, D. L., Heuveline, V. & Dössel, O. 2010 Framework for modular, flexible and efficient solving the cardiac bidomain equation using PETSc. *Math. Indus.* **15**, 363–369. (doi:10.1007/978-3-642-12110-4_55)

34 Krueger, M. W. *et al.* 2011 Alterations of atrial electrophysiology related to hemodialysis session: insights from a multiscale computer model. *J. Electrocardiol.* **44**, 176–183. (doi:10.1016/j.jelectrocard.2010.11.016)

35 Murgatroyd, F., Krahn, A. D., Yee, R., Skanes, A. & Klein, G. J. 2002 *Handbook of cardiac electrophysiology: a practical guide to invasive EP studies and catheter ablation*. London, UK: Remedica Publishing.

36 Mitchell, C. C. & Schaffer, D. G. 2003 A two current model for the dynamics of cardiac membrane. *Bull. Math. Biol.* **65**, 767–793. (doi:10.1016/S0092-8240(03)00041-7)

37 Peyrat, J.-M., Sermesant, M., Pennec, X., Delingette, H., Xu, C., McVeigh, E. R. & Ayache, N. 2007 A computational frame-work for the statistical analysis of cardiac diffusion tensors: application to a small database of canine hearts. *IEEE Trans. Med. Imag.* **26**, 1500–1514. (doi:10.1109/TMI.2007.907286)

38 Relan, J., Chinchapatnam, P. h., Sermesant, M., Rhode, K., Delingette, H., Razavi, R. & Ayache, N. 2010. Coupled personalisation of electrophysiology models for simulation of induced ischemic ventricular tachycardia. *Proc. Medical Image Computing and Computer Assisted Intervention* (*MICCAI'10*), LNCS, Beijing, China, September.

39 Keller, D. U. J., Weber, F. M., Seemann, G. & Dössel, O. 2010 Ranking the influence of tissue conductivities on forward-calculated ECGs. *IEEE Trans. Biomed. Eng.* **57**, 1568–1576. (doi:10.1109/TBME.2010.2046485)

40 Schulze, W. H. W., Krueger, M. W., Jiang, Y., Rhode, K., Weber, F. M., Caulfield, D., Knowles, B. R., Razavi, R. & Dössel, O. 2010 Localization of the atrial excitation origin by reconstruction of time-integrated transmembrane voltages. *Biomed. Techn./Biomed. Eng.* **55**, 1–237.

41 Rudy, Y. 2010 Noninvasive imaging of cardiac electrophysiology and arrhythmia. *Ann. N Y Acad. Sci.* **1188**, 214–221. (doi:10.1111/j.1749-6632.2009.05103.x)

42 McCormick, M., Nordsletten, D. A., Kay, D. & Smith, N. P. In press. Modelling left ventricular function under assist device support. *Int. J. N. Comp. Meth. Biomed.*

43 Nordsletten, D. A., Kay, D. A. & Smith, N. P. 2011 A nonconforming monolithic finite element method for problems of coupled mechanics. *Comput. Phys.* **229**, 7571–7593. (doi:10.1016/j.jcp.2010.05.043)

44 Nordsletten, D. A., Niederer, S. A., Nash, M. P., Hunter, P. J. & Smith, N. P. 2011 Coupling multi-physics models to cardiac mechanics. *Prog. Biol. Phys. Mol. Biol* **104**, 77–88.

45 Nordsletten, D., Hunter, P. & Smith, N. 2010 Conservative arbitrary Lagrangian–Eulerian forms for boundary driven and ventricular flows. *Int. J. Numer. Meth. Fluids* **56**, 1457–1463. (doi:10.1002/fld.1647)

46 Spaan, J. A., Piek, J. J., Hoffman, J. I. & Siebes, M. 2006 Physiological basis of clinically used coronary hemodynamic indices. *Circulation* **113**, 446–455. (doi:10.1161/CIRCULATIONAHA.105.587196)

47 De Bruyne, B., Baudhuin, T., Melin, J. A., Pijls, N. H., Sys, S. U., Bol, A., Paulus, W. J., Heyndrickx, G. R. & Wijns, W. 1994 Coronary flow reserve calculated from pressure measurements in humans. Validation with positron emission tomography. *Circulation* **89**, 1013–1022.

48 Pijls, N. H., van Son, J. A., Kirkeeide, R. L., De Bruyne, B. & Gould, K. L. 1993 Experimental basis of determining maximum coronary, myocardial, and collateral blood flow by pressure measurements for assessing functional stenosis severity before and after percutaneous transluminal coronary angioplasty. *Circulation.* **87**, 1354–1367.

49 Piek, J. J. *et al.* 2000 Angiographical and Doppler flow-derived parameters for assessment of coronary lesion severity and its relation to the result of exercise electrocardiography. DEBATE study group. Doppler endpoints balloon angioplasty trial Europe. *Eur. Heart J.* **21**, 466–474. (doi:10.1053/euhj.1999.1871)

50 Meuwissen, M. *et al.* 2001 Role of variability in microvascular resistance on fractional flow reserve and coronary blood flow velocity reserve in intermediate coronary lesions. *Circulation* **103**, 184–187.

51 Siebes, M., Verhoeff, B. J., Meuwissen, M., de Winter, R. J., Spaan, J. A. & Piek, J. J. 2004 Single-wire pressure and flow velocity measurement to quantify coronary stenosis hemodynamics and effects of percutaneous interventions. *Circulation* **109**, 756–762. (doi:10.1161/01.CIR.0000112571.06979.B2)

52 Coggins, D. L., Flynn, A. E., Austin, R. E., Aldea, G. S., Muehrcke, D., Goto, M. & Hoffman, J. I. E. 1990 Nonuniform loss of regional flow reserve during myocardial ischemia in dogs. *Circ. Res.* **67**, 253–264.

53 Rimoldi, O. E. & Camici, P. G. 2004 Positron emission tomography for quantitation of myocardial perfusion. *J. Nucl. Cardiol.* **11**, 482–490. (doi:10.1016/j.nuclcard.2004.05.005)

54 Plein, S., Kozerke, S., Suerder, D., Luescher, T. F., Greenwood, J. P., Boesiger, P. & Schwitter, J. 2008 High spatial resolution myocardial perfusion cardiac magnetic resonance for the detection of coronary artery disease. *Eur. Heart J.* **29**, 2148–2155. (doi:10.1093/eurheartj/ehn297)

55 Smith, N. P. & Kassab, G. S. 2001 Analysis of coronary blood flow interaction with myocardial mechanics based on anatomical models. *Phil. Trans. R. Soc. Lond. A* **359**, 1251–1263. (doi:10.1098/rsta.2001.0829)

56 Smith, N. P., Pullan, A. J. & Hunter, P. J. 2000 Generation of an anatomically based geometric coronary model. *Ann. Biomed. Eng.* **28**, 14–25. (doi:10.1114/1.250)

57 Kaimovitz, B., Lanir, Y. & Kassab, G. S. 2005 Large-scale 3-D geometric reconstruction of the porcine coronary arterial vasculature based on detailed anatomical data. *Ann. Biomed. Eng.* **33**, 1517–1535 (doi:10.1007/s10439-005-7544-3)

58 Kassab, G. S., Rider, C. A., Tang, N. J. & Fung, Y. C. 1993 Morphometry of pig coronary arterial trees. *Am. J. Physiol.* **265**, H350–H365.

59 Smith, N. P. 2004 A computational study of the interaction between coronary blood flow and myocardial mechanics. *Physiol. Meas.* **25**, 863–877. (doi:10.1088/0967-3334/25/4/007)

60 Spaan, J., Kolyva, C., van den Wijngaard, J., ter Wee, R., van Horssen, P., Piek, J. & Siebes, M. 2008 Coronary structure and perfusion in health and disease. *Phil. Trans. R. Soc. A* **366**, 3137–3153. (doi:10.1098/rsta.2008.0075)

61 van den Wijngaard, J. P., Kolyva, C., Siebes, M., Dankelman, J., van Gemert, M. J., Piek, J. J. & Spaan, J. A. 2008 Model prediction of subendocardial perfusion of the coronary circulation in the presence of an epicardial coronary artery stenosis. *Med. Biol. Eng. Comput.* **46**, 421–432. (doi:10.1007/s11517-008-0314-2)

62 Lee, J. & Smith, N. P. 2008 Theoretical modeling in hemodynamics of microcirculation. *Microcirculation* **15**, 730–745. (doi:10.1080/10739680802229589)

63 Spaan, J. A. E., ter Wee, R., VanTeeffelen, J. W. G. E., Streekstra, G., Siebes, M., Kolyva, C., Vink, H., Fokkema, D. S. & VanBavel, E. 2005 Visualization of intramural coronary vasculature by an imaging cryomicrotome suggests

compartmentalization of myocardial perfusion areas. *Med. Biol. Eng. Comput.* **43**, 431–435. (doi:10.1007/BF02344722)
64 Waters, S. L. *et al.* 2011 Theoretical models for coronary vascular biomechanics: progress and challenges. *Prog. Biophys. Mol. Biol.* **104**, 49–76. (doi:10.1016/j.pbiomolbio.2010.10.001)
65 Goyal, A., van den Wijngaard, J., van Horssen, P., Grau, V., Spaan, J. & Smith, N. 2009 Intramural spatial variation of optical tissue properties measured with fluorescence microsphere images of porcine cardiac tissue. *Conf. Proc. IEEE Eng. Med. Biol. Soc.* 1408–1411.
66 van Horssen, P., Siebes, M., Hoefer, I., Spaan, J. A. & van den Wijngaard, J. P. 2010 Improved detection of fluorescently labeled microspheres and vessel architecture with an imaging cryomicrotome. *Med. Biol. Eng. Comput.* **48**, 735–744. (doi:10.1007/s11517-010-0652-8)
67 Schuster, A. *et al.* 2010 An isolated perfused pig heart model for the development, validation and translation of novel cardiovascular magnetic resonance techniques. *J. Cardiovasc. Magn. Reson.* **12**, 53. (doi:10.1186/1532-429X-12-53)
68 van den Wijngaard, J. P., van Horssen, P., ter Wee, R., Coronel, R., de Bakker, J. M., de Jonge, N., Siebes, M. & Spaan, J. A. 2010 Organization and collateralization of a subendocardial plexus in end-stage human heart failure. *Am. J. Physiol. Heart Circ. Physiol.* **298**, H158–H162. (doi:10.1152/ajpheart.00654.2009)
69 Parker, K. H. 2009 An introduction to wave intensity analysis. *Med. Biol. Eng. Comput.* **47**, 175–188. (doi:10.1007/s11517-009-0439-y)
70 Davies, J. E. *et al.* 2006 Evidence of a dominant backward-propagating 'suction' wave responsible for diastolic coronary filling in humans, attenuated in left ventricular hypertrophy. *Circulation* **113**, 1768–1778. (doi:10.1161/CIRCULATIONAHA.105.603050)
71 Kolyva, C., Spaan, J. A., Piek, J. J. & Siebes, M. 2008 Windkesselness of coronary arteries hampers assessment of human coronary wave speed by single-point technique. *Am. J. Physiol. Heart Circ. Physiol.* **295**, H482–H490. (doi:10.1152/ajpheart.00223.2008)
72 Siebes, M., Kolyva, C., Verhoeff, B. J., Piek, J. J. & Spaan, J. A. 2009 Potential and limitations of wave intensity analysis in coronary arteries. *Med. Biol. Eng. Comput.* **47**, 233–239. (doi:10.1007/s11517-009-0448-x)
73 Rosenthal 2005 Coarctation of the aorta from fetus to adult: curable condition or life long disease process? *Heart* **91**, 1495–1502. (doi:10.1136/hrt.2004.057182)
74 Giordano, U., Cifra, B., Giannico, S., Turchetta, A. & Calzolari, A. 2009 Mid-term results, and therapeutic management, for patients suffering hypertension after surgical repair of aortic coarctation. *Cardiol. Young* **19**, 451–455. (doi:10.1017/S1047951109990734)
75 Ladisa, J. F., Taylor, C. A. & Feinstein, J. A. 2010 Aortic coarctation: recent developments in experimental and computational methods to assess treatments for this simple condition. *Prog. Pediatr. Cardiol.* **30**, 45–49. (doi:10.1016/j.ppedcard.2010.09.006)
76 Kim, H. J., Vignon-Clementel, I. E., Figueroa, C. A., LaDisa, J. F., Jansen, K. E., Feinstein, J. A. & Taylor, C. A. 2009 On coupling a lumped parameter heart model and a three-dimensional finite element aorta model. *Ann. Biomed. Eng.* **37**, 2153–2169. (doi:10.1007/s10439-009-9760-8)
77 Stewart, S. F. C. *et al.* 2009 Preliminary results of FDA's 'Critical Path' project to validate computational fluid dynamic methods used in medical device evaluation (abstract). *ASAIO J* **55**, 173.
78 Radaelli, A. G. *et al.* 2008 Reproducibility of haemodynamical simulations in a subject-specific stented aneurysm model—a report on the Virtual Intracranial Stenting Challenge 2007. *J. Biomech.* **41**, 2069–2081. (doi:10.1016/j.jbiomech.2008.04.035)

GLOSSARY

Alphabetical list of abbreviations

AF	atrial fibrillation
APD	action potential duration
BSPM	body surface potential mapping
CAD	coronary artery disease
CRT	cardiac resynchronization therapy
CT	computed tomography
ECG	electrocardiogram
ECGI	electrocardiographic imaging
FE	finite element
HD	haemodialysis
IVC	inferior vena cava
LIPV	left inferior pulmonary vein
LSPV	left superior pulmonary vein
LV	left ventricle
LVAD	left ventricular assist device
MR	magnetic resonance
MRI	magnetic resonance imaging
RFA	radiofrequency ablation
RIPV	right inferior pulmonary vein
RSPV	right superior pulmonary vein
SVC	superior vena cava
VT	ventricular tachycardia